Investigating the Chromospheric Footpoints of the Solar Wind

Paul Bryans[1] , Scott W. McIntosh[1] , David H. Brooks[2] , and Bart De Pontieu[3,4,5]

[1] National Center for Atmospheric Research, High Altitude Observatory, P.O. Box 3000, Boulder, CO 80307, USA; pbryans@ucar.edu
[2] College of Science, George Mason University, 4400 University Drive, Fairfax, VA 22030, USA
[3] Lockheed Martin Solar & Astrophysics Laboratory, Palo Alto, CA 94304, USA
[4] Rosseland Center for Solar Physics, University of Oslo, P.O. Box 1029 Blindern, NO-0315, Oslo, Norway
[5] Institute of Theoretical Astrophysics, University of Oslo, P.O. Box 1029 Blindern, NO-0315, Oslo, Norway

Abstract

Coronal holes present the source of the fast solar wind. However, the fast solar wind is not unimodal—there are discrete, but subtle, compositional, velocity, and density structures that differentiate different coronal holes as well as wind streams that originate within one coronal hole. In this Letter we exploit full-disk observational "mosaics" performed by the Interface Region Imaging Spectrograph (IRIS) spacecraft to demonstrate that significant spectral variation exists within the chromospheric plasma of coronal holes. The spectral differences outline the boundaries of some—but not all—coronal holes. In particular, we show that the "peak separation" of the Mg II h line at 2803 Å illustrates changes in what appear to be open magnetic features within a coronal hole. These observations point to a chromospheric source for the inhomogeneities found in the fast solar wind. These chromospheric signatures can provide additional constraints on magnetic field extrapolations close to the source, potentially on spatial scales smaller than from traditional coronal hole detection methods based on intensity thresholding in the corona. This is of increased importance with the advent of Parker Solar Probe and Solar Orbiter and the ability to accurately establish the connectivity between their in situ measurements and remote sensing observations of the solar atmosphere.

Unified Astronomy Thesaurus concepts: Quiet solar chromosphere (1986); Solar magnetic fields (1503); Solar coronal holes (1484); Solar corona (1483)

1. Introduction

First routinely observed with the advent of space-based instruments, coronal holes (CHs) are among the most conspicuous of features in EUV and X-ray solar images. Identified as regions of low intensity, they appear largely homogeneous over their extent, which can cover an appreciable fraction of the solar surface. Photospheric observations show that the magnetic field associated with CHs is more uniform and unipolar than the surrounding quiet Sun (QS; e.g., Levine 1982), and extrapolation of the photospheric field to the heliosphere provides evidence that CHs are connected to open-field solar wind streams. Flux tubes are thought to expand superradially and ultimately connect the outflowing CH plasma to the high-speed solar wind (e.g., Wilcox & Howard 1968). The amount of open flux, however, is underestimated by the extrapolations (Linker et al. 2017) indicating that our understanding of the precise connection between CHs and the solar wind is incomplete.

In addition to the obvious space weather implications, tracing the solar wind back to its source has recently risen in importance with the launch of Parker Solar Probe (PSP; Fox et al. 2016) and Solar Orbiter (SolO; Müller et al. 2013). Successful coordination of the in situ instruments of these missions with complementary solar-observing instruments is contingent on an accurate extrapolation of the magnetic field from the solar surface to the spacecraft. Further, the extreme telemetry demands and eccentric orbits that result in short observational windows, make it critical to successfully coordinate with ground- and space-based instruments to maximize scientific output. Early results from PSP have shown the solar wind emanating from CHs to be more structured than previously thought, including ubiquitous switchbacks of the

magnetic field (Bale et al. 2019). This structure is largely washed out by the time the solar wind reaches the Earth, but remains detectable at the closer heliocentric distance of PSP. One is thus led to question whether the CHs from which this solar wind derives are as homogeneous as their EUV signatures suggest.

There exist several algorithms to detect CHs (e.g., Krista & Gallagher 2009; Reiss et al. 2015; Heinemann et al. 2019). The observational inputs and segmentation methods of these differ, but are all based to some extent on intensity thresholding of coronal EUV images. While EUV intensity is a strong indication of CH location, it also poses some challenges. Distinguishing CHs from QS based on an intensity threshold is inherently arbitrary in nature. Further, the wavelength of the EUV emission is dependent on the temperature (and hence the location) of the emitting plasma, so techniques based on observations of different wavelengths will determine the CH boundary at different heights in the atmosphere, resulting in differing CH sizes as the magnetic field lines expand with distance from the surface. A compounding issue is the fact the EUV emission is optically thin in the corona, so that the viewing angle of any CH will alter its appearance due to superposition of emission along the line of sight. Measurements of CHs lower in the atmosphere may allow one to overcome these ambiguities.

In contrast to their stark observational signature in the corona, CHs are difficult to distinguish from the surrounding QS in the photosphere and chromosphere. Absorption by He I 10830 Å shows CHs in the upper chromosphere, and the intensity distribution outside CHs is slightly broader than that inside CHs in chromospheric Ca II K (Marsh 1977), but CHs are generally difficult to detect in the lower solar atmosphere by

intensity measurements. Spectral data can, however, discriminate where intensity cannot.

Peter (1999) showed CHs to exhibit increased line shifts and widths compared to QS in He I 584 Å. In a study of Ca II H and K lines, Teplitskaya et al. (2007) found that the spectral signature of these lines differs from CH to QS. In particular, the self-reversal of these double-peaked lines was found to differ not just from CH to QS, but to have structure *within* a CH that is related to the chromospheric network. Evidence of this structure imprinting on the solar wind can be found in Solar Ultraviolet Measurements of Emitted Radiation (SUMER; Wilhelm et al. 1995) observations, which indicate that the faster outflowing velocities emanate from the chromospheric magnetic network (Hassler et al. 1999). It seems, then, that high-resolution, spectrally resolved observations of the chromosphere could be crucial in properly understanding the nature of the solar wind.

Recent observational work on the nature of CHs in the chromosphere has resulted in some interesting, if inconclusive, findings. Emission measurements of Mg II h and k, not possible from the ground, became available from space with the Interface Region Imaging Spectrograph (IRIS; De Pontieu et al. 2014) in 2013, providing diagnostic information of the photosphere and chromosphere. In a comprehensive study of how these lines vary across solar features, Lacatus (2018) found it generally difficult to distinguish CHs from QS but reported a measurable increased Mg II k line width in CH spectra compared to the QS. Kayshap et al. (2018) also studied the spectral differences in Mg II k from CH to QS, reporting that the intensity of the k3 spectral feature is lower in CHs than the surrounding QS for similar magnetic field strength. Both of these studies were limited to a handful of observations with a limited field of view and did not address the connection between CHs and the solar wind.

In this Letter, we utilize IRIS observations of the full Sun to build up a comprehensive picture of CHs in the lower solar atmosphere. In this way, we can investigate the spectral signatures of CHs across the entire disk and compare with the emission from other parts of the Sun at the same time. These large fields of view are also used to show spectral differences within CHs. The results have clear implications for diagnoses of the solar wind and connecting PSP and SolO in situ measurements with the solar surface.

2. Observations

The Interface Region Imaging Spectrograph (IRIS) satellite has observed spectra from CHs since it was launched in 2013. The spectrograph slit is $175''$ long, while CHs typically span several hundred arcseconds. Measuring the spectrum for an entire CH, then, is usually only possible by tessellating the IRIS field of view over a larger area. IRIS has a full-Sun mosaic observing sequence that achieves this goal. This synoptic mode has been run on a monthly basis (outside the eclipse season of November to February) since September 2013. There are now over 70 full-disk mosaics, providing comprehensive data on the chromospheric and transition region spectra of CHs over the entire solar disk and a significant fraction of the solar cycle.

Each of the mosaics comprises 185 pointings to cover the entire solar disk, with a total duration of ~18 hr including time taken to repoint the satellite. At each pointing a $128'' \times 175''$ raster, with spatial sampling of $2''$ and $0.''35$ in x and y,

respectively, and 1–2 s (and occasionally up to 8 s) exposure time, is taken around the six strongest spectral features of the IRIS wavelength range (Mg II h and k, C II 1334 Å and 1335 Å, and Si IV 1393 Å and 1403 Å). All IRIS full-disk mosaics have been coaligned and made available in FITS format on the IRIS website.[6]

2.1. Mg II Line Profile Fitting

The strongest emission features measured by the IRIS spectrograph are the Mg II h and k lines at 2803 and 2796 Å. Their formation spans a range of heights from the photosphere to chromosphere, making them of excellent diagnostic value when exploring CHs lower in the atmosphere than they are typically measured. The formation properties are complex, however, and require careful modeling to translate spectral signatures to physical properties of the plasma. Using synthetic spectra from 3D MHD simulations, several works have demonstrated a correlation between the spectral characteristics and the temperature and velocities throughout the formation height of the lines (Leenaarts et al. 2013a, 2013b; Pereira et al. 2013). The ability to diagnose any of these physical properties from actual observations first requires that we quantify certain aspects of the spectral features.

The spectral profiles of the optically thick Mg II lines are generally double peaked. We choose to fit the line with a double Gaussian profile as described in Schmit et al. (2015) and Bryans et al. (2016), where one can also find example profiles of the line. This allows us to identify the spectral features h3 (wavelength and intensity of the central reversal), h2v (blue peak), and h2r (red peak). A first analysis of the statistical variation of the Mg II h profile using a full-disk mosaic was performed by Schmit et al. (2015), which focused on how the spectra vary with photospheric magnetic field strength across the disk. Here, rather, we investigate the spectral character of CHs in comparison to neighboring QS, with particular attention paid to the "peak separation," i.e., the distance between the h2v and h2r peaks. This quantity is generally interpreted as a measure of chromospheric opacity and velocity gradients in the region of formation (Leenaarts et al. 2013b; Pereira et al. 2013); we discuss the physical significance of the shape of the Mg II h profile in greater detail in Section 4.

2.2. Full-disk Mosaics

Identification of CHs is typically achieved using a combination of coronal EUV images and photospheric magnetograms, where EUV intensity identifies the CH and unipolarity discriminates them from other dim features such as filament channels. Here, we choose to utilize Atmospheric Imaging Assembly (AIA; Lemen et al. 2012) and Helioseismic and Magnetic Imager (HMI; Schou et al. 2012) observations from the Solar and Dynamics Observatory (SDO; Pesnell et al. 2012) for their high cadence and full-Sun coverage. The best fidelity in comparing data from the different instruments is attained by isolating parts of the AIA and HMI fields of view that match the timing of the IRIS rasters. Thus, we collect the AIA and HMI images closest in time for each IRIS pointing, coalign them, and crop the AIA/HMI image to the same field of view as IRIS. These subimages are then composed into full-disk
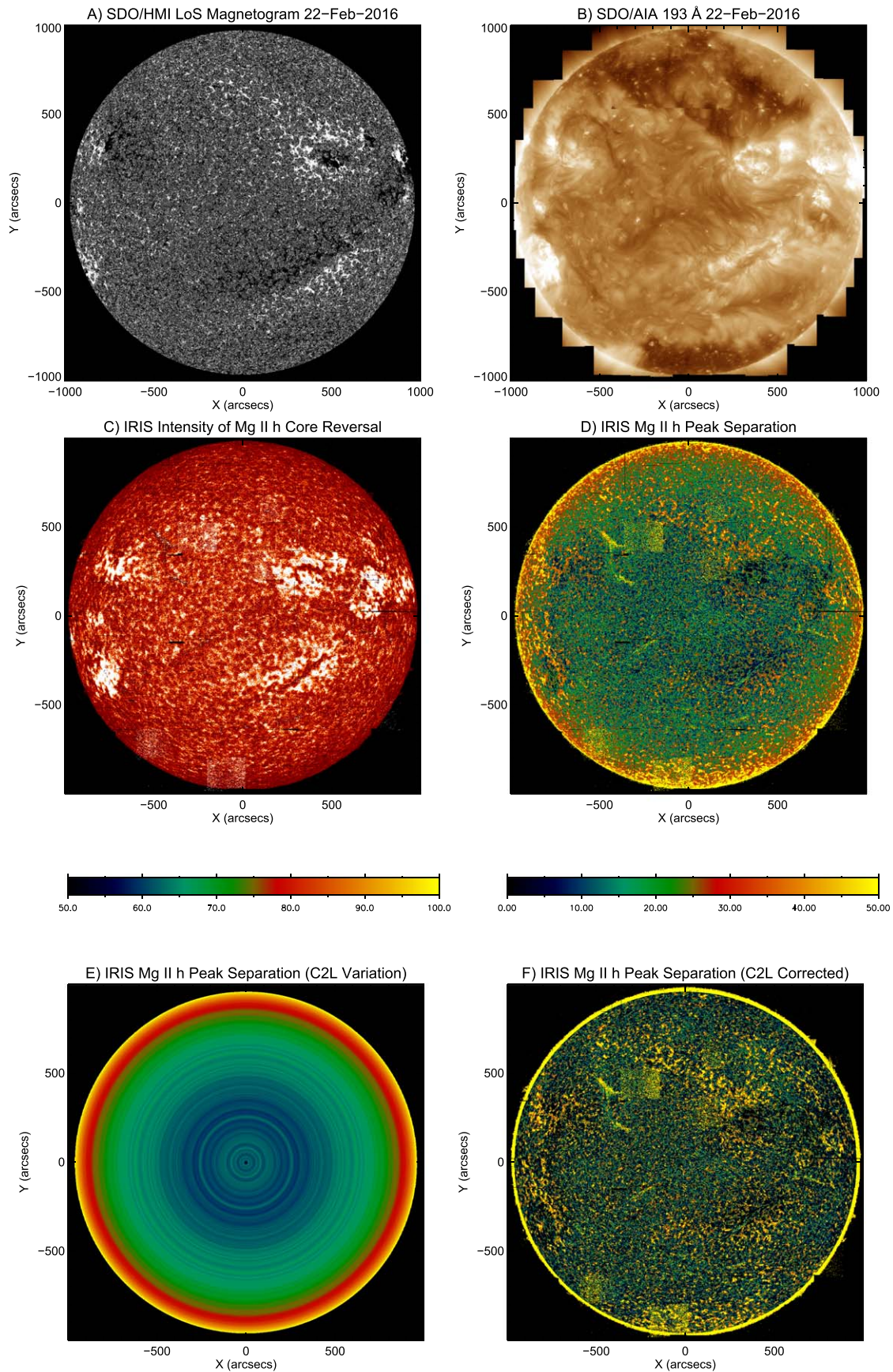
---

[6] https://iris.lmsal.com/mosaic.html

Figure 1. SDO and IRIS full-disk observations from 2016 February 22. The HMI (A) and AIA (B) Frankenmaps are constructed of subimages with the same fields of view and timing of the IRIS rasters that comprise the mosaic. The CHs in the northern hemisphere and at the south pole are most evident in the AIA intensity image (B), but not in Mg II intensity (C). The CHs are evident, however, in the Mg II peak separation map (D). After removing the center-to-limb variation, this is even clearer (F). (The small area of increased intensity/peak separation at the south pole is an artifact caused by cosmic-ray hits.)
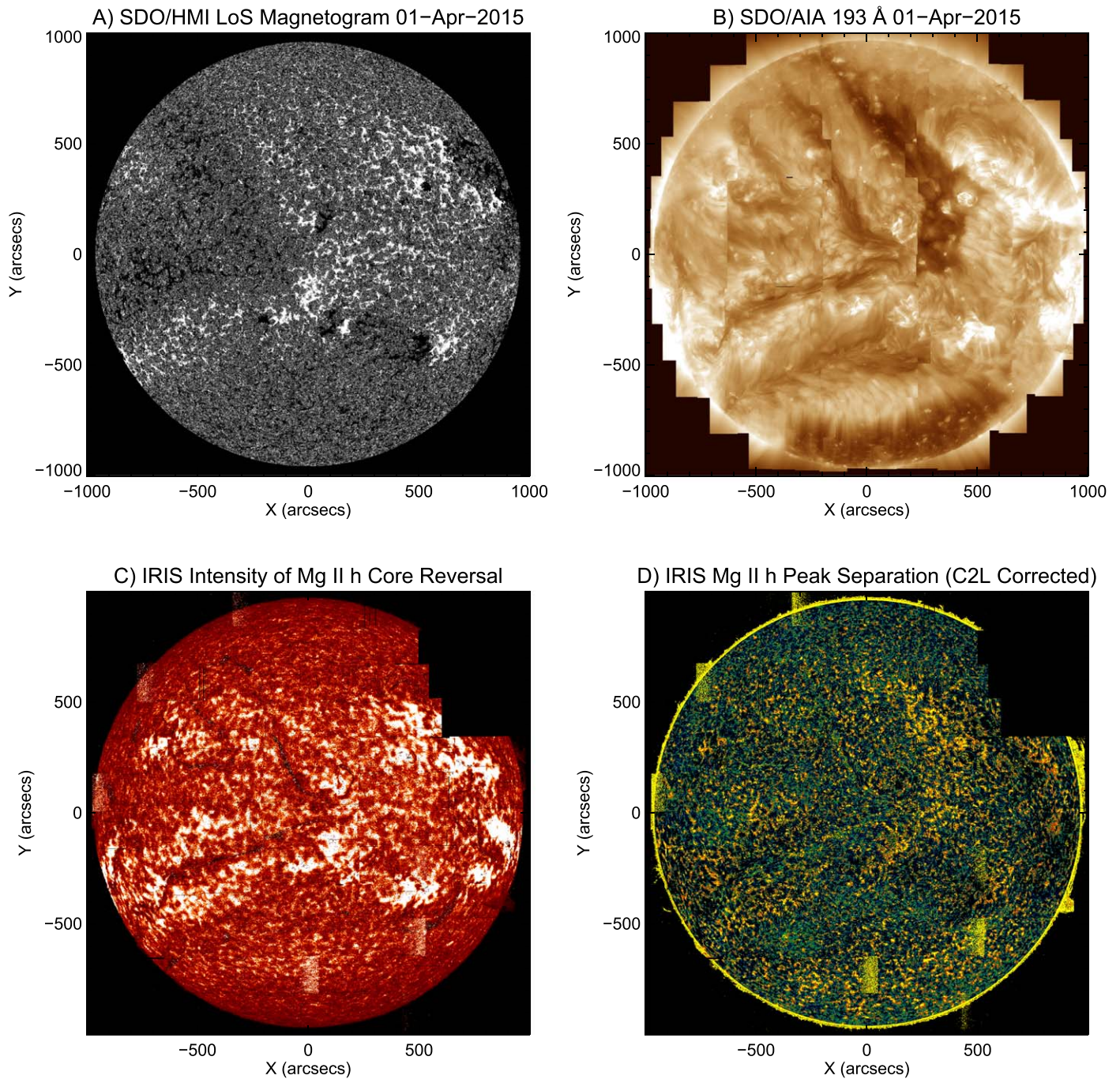
Figure 2. SDO and IRIS full-disk observations from 2015 April 1. The line-of-sight magnetogram is shown in panel (A), 193 Å intensity in panel (B), Mg II intensity in panel (C), and Mg II peak separation (after center-to-limb removal) in panel (D). A dropout during these observations resulted in some data loss, but it does not correspond to the CH locations.

images that we have termed "Frankenmaps" (available in FITS format on the IRIS website; see footnote 6).

From the several tens of full-disk mosaics in the IRIS archive, the majority have CHs in their fields of view. The size and locations of these CHs vary from mosaic to mosaic, and we have selected a small subset of mosaics with CHs covering a range of extents and locations (Figures 1–3). These were chosen for illustrative purposes, showing both polar and equatorial CHs and the influence of neighboring active regions on the peak separation measure. The findings of these three examples are representative of the entire sample.

Figure 1 shows observations from 2016 February 22. Panels (A) and (B) show the HMI and AIA Frankenmaps for the same times as the IRIS mosaic, showing the line-of-sight magnetic field and the 193 Å intensity, respectively. The two CHs are most apparent in panel (B), with a southern polar CH and a more extended CH in the northern hemisphere. The Mg II intensity, shown in panel (C), does not show any immediately obvious indications of the CHs. Only when looking at an image of the peak separation do the CHs begin to appear in the Mg II observations. The northern CH is seen clearly in the peak separation map of panel (D). However, the peak separation has
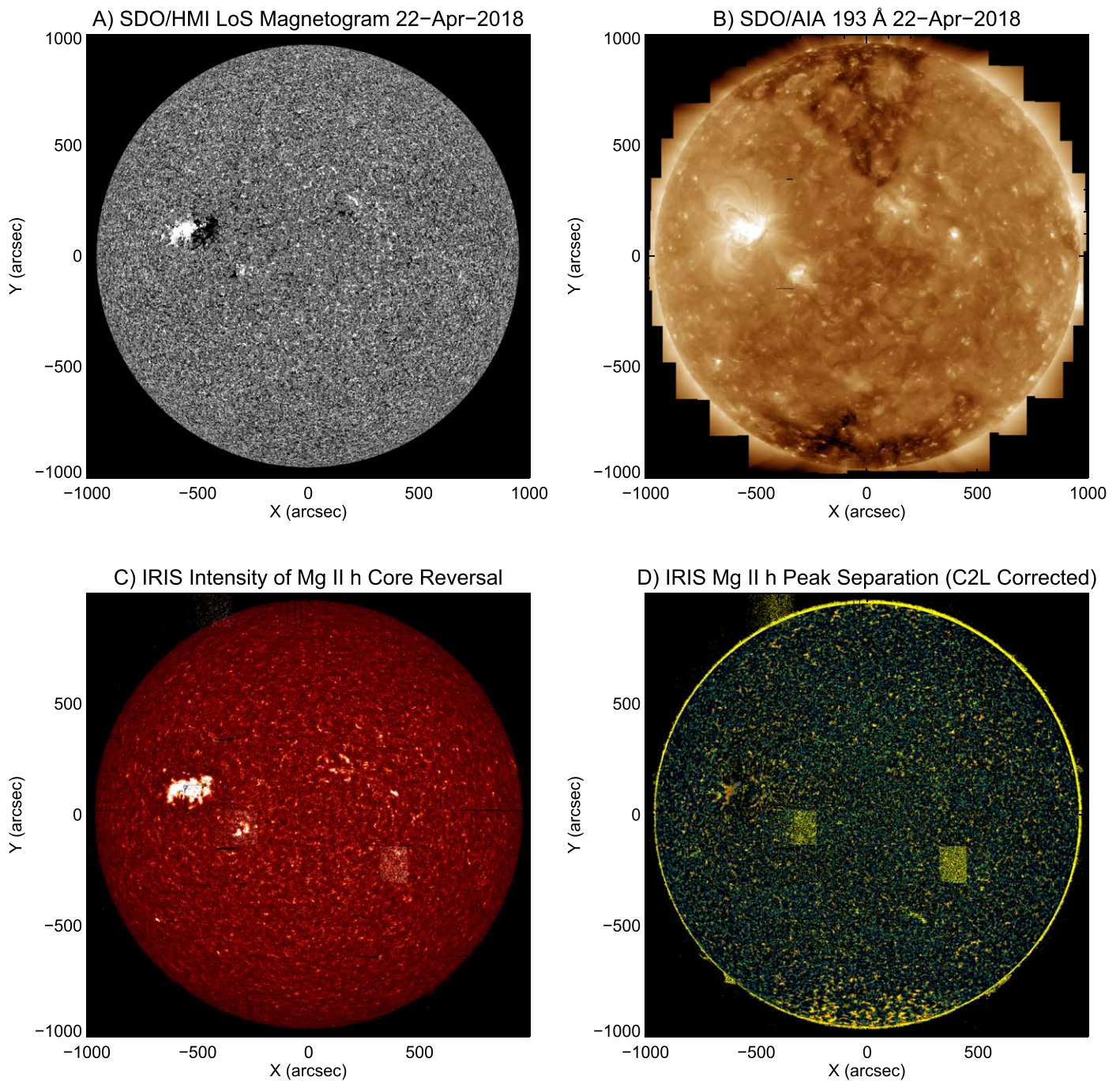
Figure 3. SDO and IRIS full-disk observations from 2018 April 22. The line-of-sight magnetogram is shown in panel (A), 193 Å intensity in panel (B), Mg II intensity in panel (C), and Mg II peak separation (after center-to-limb removal) in panel (D). (The rectangular areas of increased intensity/peak separation near disk center are artifacts caused by cosmic-ray hits.)

a strong dependency on viewing angle, making it difficult to discriminate the southern CH. For each mosaic, we calculated this center-to-limb variation (shown in panel (E)) by taking the mean peak separation of concentric QS annuli, i.e., excluding CHs and ARs that have enhanced peak separations. This mean radial value has been removed from the peak separation to produce a corrected peak separation map, shown in panel (F).

The difference in panels (C) and (F) of Figure 1 are striking. There are clear indications of both CHs in the peak separation image, where none was apparent in the Mg II intensity. The delineation of the CH by this measure is not always as obvious as in the EUV intensity, such as is shown in panel (B). In this

mosaic example, for instance, the polar CH in the south is clearly distinguished by the peak separation. The northern CH is less clearly so. In this case, the southern region of the CH is clearly identified by an increased peak separation, while the polar region appears more patchy. This leads to the presumption that the Mg II peak separation distinguishes aspects of CHs that coronal intensity does not.

Figures 2 and 3 show two more examples of mosaics that capture CHs, on 2015 April 1 and 2018 April 22, respectively. We show the HMI line-of-sight magnetogram, the AIA 193 Å intensity, and Mg II intensity and center-to-limb-removed peak separation in panels (A), (B), (C), and (D) of these figures. In

Figure 2, we again have a southern polar CH and an equatorial CH in the northern hemisphere. The equatorial CH does show an increased peak separation but, like that of Figure 1, it does not demark its entire breadth. Rather, only the eastern and southern regions of the CH show a marked increase in peak separation from the surrounding QS. Of the two CHs in Figure 3, one shows a clear enhancement in peak separation (southern CH) and the other does not (northern CH).

Figure 3 shows an example of a mosaic with a large active region (AR) in addition to CHs. The Mg II peak separation is strongly affected by the AR. Unlike the CH signature, however, there is both an increase and decrease in the peak separation in the vicinity of the AR. Such a signature in the AR is to be expected given that the peak separation is known to be a measure of chromospheric opacity and velocity gradients (Leenaarts et al. 2013b; Pereira et al. 2013). The important point for the current discussion is that an increase in the Mg II peak separation is not a unique identifier of a CH.

To better highlight the colocation of enhanced peak separation and CHs, Figure 4 shows the same peak separation images of Figures 1–3 with the CH locations overplotted. These are shown in the leftmost panels of Figure 4. The CH contours plotted here in red were determined by a simple thresholding of the AIA 193 Å intensity. A notable exception to the correlation of peak separation and CH is seen in the mosaic of 2016 February 22 (the top left panel of Figure 4). In this case, the area of enhanced peak separation corresponding to the northern CH extends farther south than the CH boundary. This is because of the abutting AR at this location, which also results in an increase in the peak separation. Like the AR of Figure 3, one observes areas of both increased and decreased peak separation at the AR location.

The rightmost panels of Figure 4 show histograms of the peak separation within the CH regions compared to the rest of the solar disk. In all cases the histograms representing CHs are shifted to higher values, indicating a larger peak separation in CHs than elsewhere on the disk.

3. High-resolution Observations

The full-disk mosaics that have formed the observational basis of the Letter thus far are not run at the spatial resolution limit of IRIS. To keep the mosaic to within 18 hr the raster scans with a slit step of 2″, rather than the maximum resolution of 0″.35, and is spatially binned to a resolution of 2″ along the slit. To complement the full coverage of the mosaics we turn to higher-resolution observations of smaller regions of CHs. Using these high-resolution data allows us to investigate the spatial correlation of the structure of the peak separation enhancement with respect to the chromospheric network. We have chosen three CH observations that show this correlation for different projection angles.

Panels (A), (B), and (C) of Figure 5 show CH observations in the northern hemisphere, disk center, and near the south pole, respectively. In each panel the integrated Mg II h intensity (2803–2804 Å) is plotted in gray color scale, with the peak separation overplotted in red contours. In each example, the increased peak separation follows the bright chromospheric network. There is an offset, however, based on the viewing angle. The peak separation enhancement follows the network at disk center (panel (B)), but is to the north of it in the northern hemisphere (panel (A)), and similarly to the south at the south pole (panel (C)). This suggests that the enhanced peak

separation is an indicator of a feature higher in the atmosphere than the integrated intensity.

Spicules offer a logical explanation for the relation between the enhanced peak separation and intensity. At the photospheric level, magnetic flux is pushed to the boundary of super-granules, resulting in the chromospheric network. For similar reasons, these locations are also the footpoints of spicules, which extend higher in the atmosphere in CHs than in the QS (Beckers 1968). Spicules are known to exhibit broad double-peaked Mg II profiles in CHs at the limb, caused by the superposition of many spicules along the line of sight (Pereira et al. 2014). For CHs closer to disk center, spicules may also result in broader lines due to their increased opacity because they extend higher into the atmosphere than they do in the QS. This is consistent with the findings of Lacatus (2018), who measured increased Mg II opacity in the chromospheric network compared to the internetwork. Observations of the broad spicular profiles in relation to the chromospheric network, then, depend on the viewing angle. Near disk center, when viewed directly from above, the spicules and network appear colocated. Closer to the limb, projection effects mean the spicules will appear offset from the network because of their extended height. These effects will also depend, to some extent, on the magnetic field direction. The exact extent of the offset between the chromospheric network and the spicules will be a function of both the location on the disk and how the magnetic field differs from radial.

4. Discussion

IRIS full-disk mosaics reveal a discernible difference in the spectral characteristics between CHs and QS in the chromosphere. The mosaics, in conjunction with the Frankenmaps of SDO, illuminate the chromospheric CH signatures on a solar scale that is not readily apparent from analyses of smaller fields of view. The full-Sun scans also reveal differences both within and between CHs. Within a CH there is a division of regions with and without enhanced peak separations, while other CHs do not show any such enhancement. In the areas that do have an enhanced peak separation, it forms a network-like structure.

This structure is most likely an effect of spicules within the CH. They have been observed to have broad, large peak-separated profiles of Mg II in CHs at the limb (Tei et al. 2020). They are known to preferentially form around the chromo-spheric network, at the boundaries of supergranules, where increased Mg II opacity has been measured (Lacatus 2018). And their extension higher into the atmosphere than the chromospheric network explains the projection effects seen between the enhanced peak-separated profiles and the network seen in intensity.

The partition of CHs into areas with and without an enhancement of their peak separation is of particular interest since it characterizes in a way that neither the spectrally unresolved intensity of the chromosphere nor corona does. It confirms the idea that the magnetic structure of CHs is less homogeneous in the chromosphere, before expanding into the corona (e.g., Cranmer 2009). It also implies that differences in the magnetic field connectivity are found low in the atmosphere, where spicules cause an increase in chromospheric opacity. We speculate that the regions with enhanced peak separation indicate "open" radial field that allow spicules to extend in height above those found in either the QS or the nonenhanced peak separation regions of CHs.
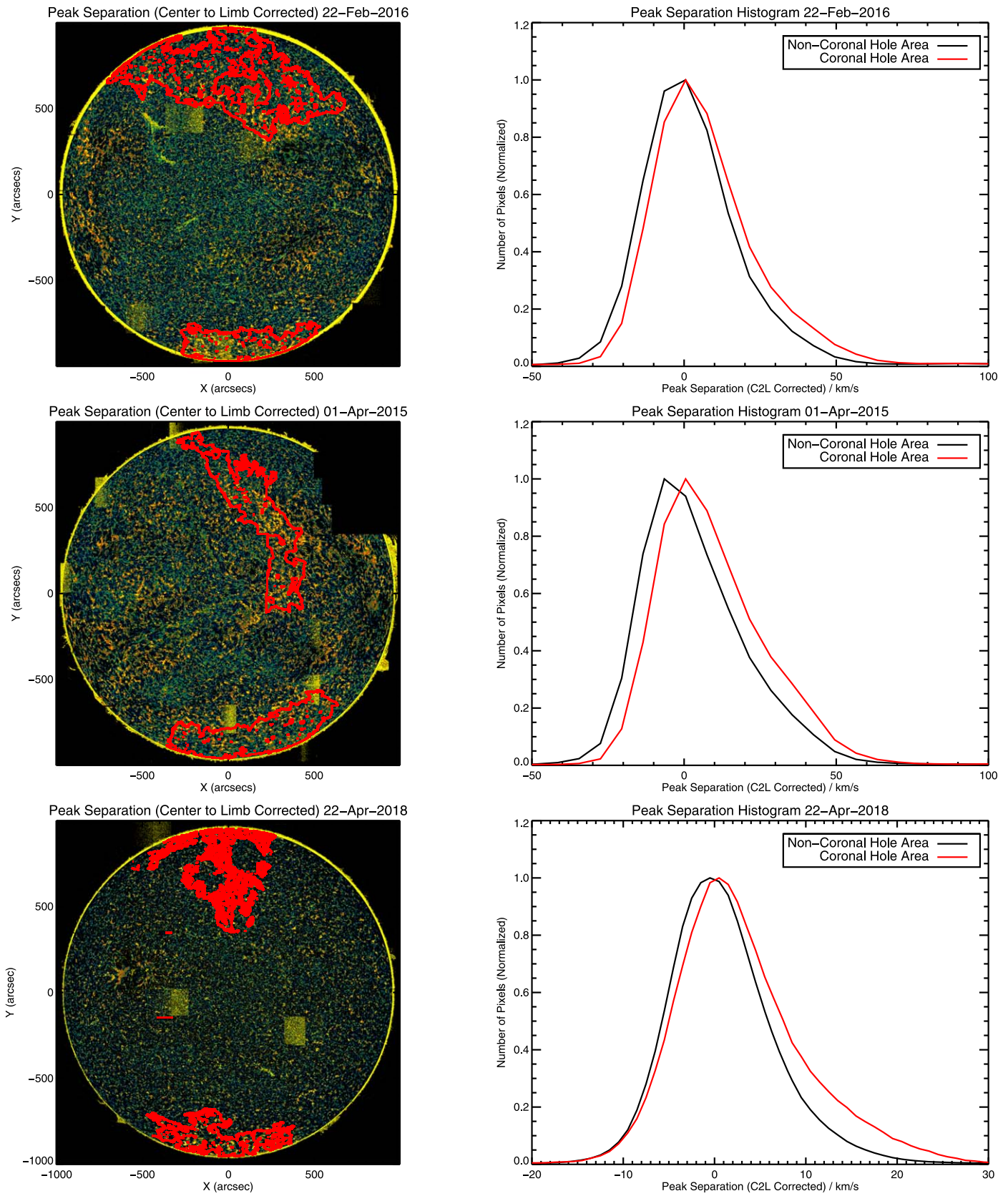
Figure 4. Coronal hole contours based on AIA 193 Å intensity thresholds overplotted on the peak separation maps of the three mosaics (left). The right panels show histograms of the peak separation within and without the CHs.
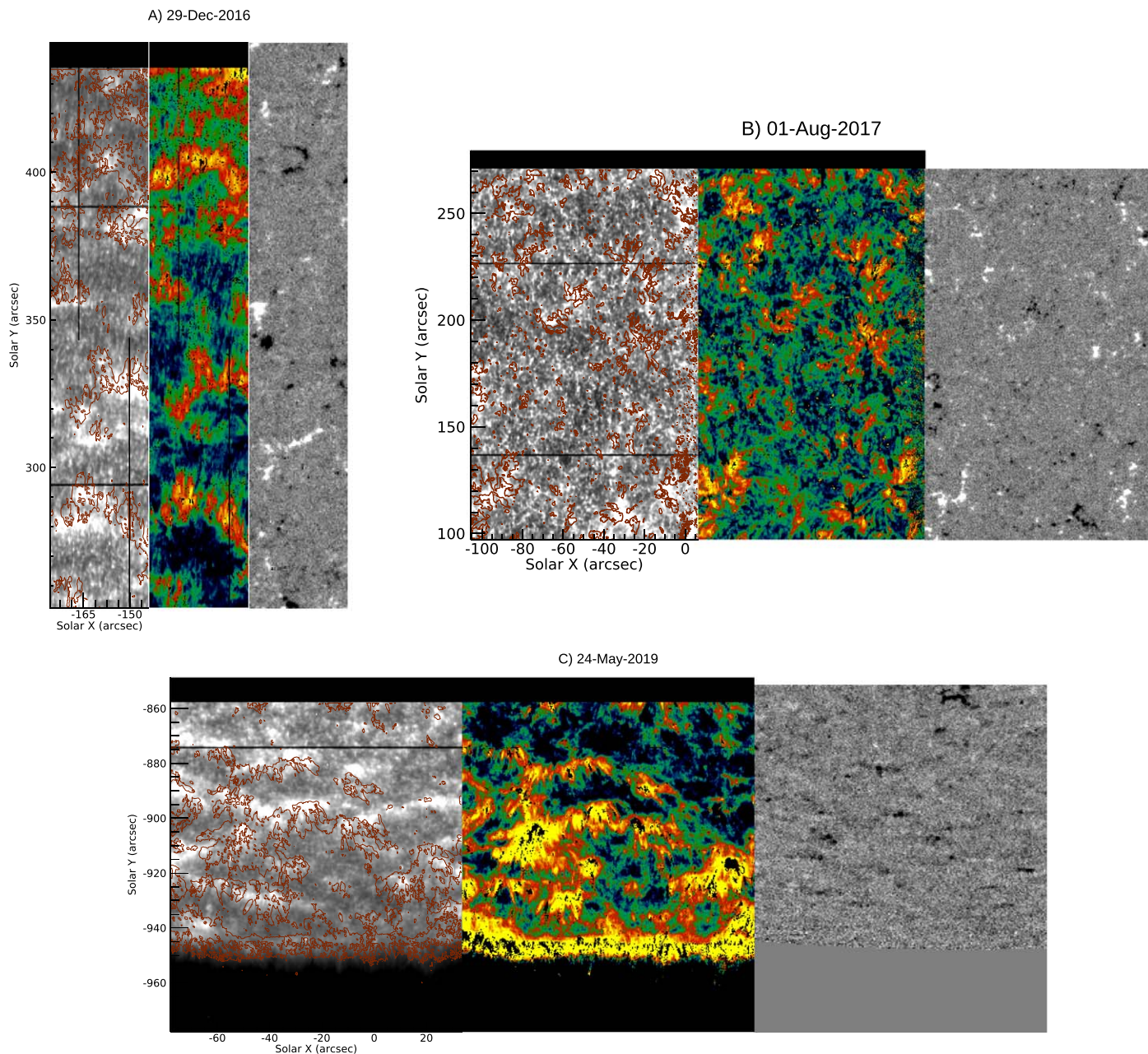
Figure 5. High-resolution CH observations in the northern hemisphere (A), disk center (B), and southern hemisphere (C). For each location the integrated Mg II h intensity is shown in gray scale on the left, the peak separation in color in the center, and the HMI line-of-sight magnetogram on the right. To better indicate the correlation, the peak separation is also overplotted in red contours on the intensity image.

There also arise questions on the nature of the chromosphere that lead to these two distinct regions. Interpreting the optically thick spectra of Mg II to determine the physical characteristics of the plasma, however, can be challenging. Previous work suggests that both velocity gradients and increased opacity can lead to increased peak separation. It is unclear which of these effects dominates our results. To determine this, we can exploit recent innovations in modeling the formation of the Mg II lines. The Stockholm Inversion Code (STiC; de la Cruz Rodríguez et al. 2019) is the first to study the lines of the upper chromosphere—including Mg II—while including non-LTE and partial redistribution (PRD) effects and a stratified model atmosphere. Deriving realistic physical parameters based on the IRIS spectra is now possible. Building on the STiC framework, and adding machine- and deep-learning techniques, is the IRIS[2]

code (Sainz Dalda et al. 2019). While STiC requires many CPU hours to invert a single IRIS pixel, IRIS[2] can return a robust model atmosphere for an entire IRIS mosaic in a fraction of the time. We thus have a powerful tool for exploring what atmospheric conditions lead to the spectral profiles observed in CHs, and determining if profiles from globally open and locally closed magnetic features vary as dramatically as suggested in the present work. This will be the subject of a follow-up paper. Such work will help to address which physical conditions lead to the increased peak separation. This is likely critical to better understand why some CH regions show increased peak separation and others do not. For example, if the increased peak separation occurs in spicules because of the increased turbulence or wave motions in the direction perpendicular to the magnetic field, one would expect the peak separation to

depend on, in part, the angle between the magnetic field and line of sight, meaning viewing angle perhaps plays an important role.

For the CHs presented here, the EUV intensity of coronal emission does not always follow the pattern of the Mg II peak separation. In much the same way that the spectral shape of the chromospheric emission highlights differences that its intensity does not, one can postulate that the spectral characteristics of the coronal emission may show variation across a CH where the intensity (such as observed by AIA) appears uniform. How the chromospheric pattern of varying Mg II peak separation impacts the corona remains an open question, but one that can be answered with coordinated coronal and chromospheric spectroscopy. The Extreme Ultraviolet Imaging Spectrometer (EIS; Culhane et al. 2007) on board Hinode (Kosugi et al. 2007) would be the ideal instrument to make such a study. While AIA is a broadband imager that only measures EUV intensity, EIS is a spectrometer with high spectral resolution of coronal emission lines that span a range of coronal temperatures. Like IRIS, its field of view is limited but, also like IRIS, it can observe the entire solar disk by mosaicking several pointings. An example of the EIS full-Sun scans is shown in Brooks et al. (2015), and these observations are now regularly coordinated with the IRIS mosaics. We intend to present the results of a study combining IRIS and EIS observations in a forthcoming publication.

The accurate mapping of solar features from the surface, through the Sun's atmosphere, and ultimately to the Earth has long been a goal of the heliophysics community. CHs, as sources of the fast solar wind, are of particular interest because of their space weather impact. And the recent launch of PSP and SolO adds to the importance of accurately tracing the solar wind, from points not necessarily on the Sun–Earth line, back to its source regions. The results of this Letter reveal substructure within CHs in the lower solar atmosphere that may point to variation in the resulting solar wind. Work remains to be done, however, on tracing the effects of this substructure through the solar atmosphere and into the heliosphere.

ORCID iDs

Paul Bryans https://orcid.org/0000-0001-5681-9689
Scott W. McIntosh https://orcid.org/0000-0002-7369-1776
David H. Brooks https://orcid.org/0000-0002-2189-9313
Bart De Pontieu https://orcid.org/0000-0002-8370-952X

References

Bale, S. D., Badman, S. T., Bonnell, J. W., et al. 2019, Natur, 576, 237
Beckers, J. M. 1968, SoPh, 3, 367
Brooks, D. H., Ugarte-Urra, I., & Warren, H. P. 2015, NatCo, 6, 5947
Bryans, P., McIntosh, S. W., De Moortel, I., & De Pontieu, B. 2016, ApJL, 829, L18
Cranmer, S. R. 2009, LRSP, 6, 3
Culhane, J. L., Harra, L. K., James, A. M., et al. 2007, SoPh, 243, 19
de la Cruz Rodríguez, J., Leenaarts, J., Danilovic, S., & Uitenbroek, H. 2019, A&A, 623, A74
De Pontieu, B., Title, A. M., Lemen, J. R., et al. 2014, SoPh, 289, 2733
Fox, N. J., Velli, M. C., Bale, S. D., et al. 2016, SSRv, 204, 7
Hassler, D. M., Dammasch, I. E., Lemaire, P., et al. 1999, Sci, 283, 810
Heinemann, S. G., Temmer, M., Heinemann, N., et al. 2019, SoPh, 294, 144
Kayshap, P., Tripathi, D., Solanki, S. K., & Peter, H. 2018, ApJ, 864, 21
Kosugi, T., Matsuzaki, K., Sakao, T., et al. 2007, SoPh, 243, 3
Krista, L. D., & Gallagher, P. T. 2009, SoPh, 256, 87
Lacatus, D. A. 2018, PhD Thesis, School of Mathematical Sciences, Monash Univ.
Leenaarts, J., Pereira, T. M. D., Carlsson, M., Uitenbroek, H., & De Pontieu, B. 2013a, ApJ, 772, 89
Leenaarts, J., Pereira, T. M. D., Carlsson, M., Uitenbroek, H., & De Pontieu, B. 2013b, ApJ, 772, 90
Lemen, J. R., Title, A. M., Akin, D. J., et al. 2012, SoPh, 275, 17
Levine, R. H. 1982, SoPh, 79, 203
Linker, J. A., Caplan, R. M., Downs, C., et al. 2017, ApJ, 848, 70
Marsh, K. A. 1977, SoPh, 52, 343
Müller, D., Marsden, R. G., St., Cyr, O. C., & Gilbert, H. R. 2013, SoPh, 285, 25
Pereira, T. M. D., De Pontieu, B., Carlsson, M., et al. 2014, ApJL, 792, L15
Pereira, T. M. D., Leenaarts, J., De Pontieu, B., Carlsson, M., & Uitenbroek, H. 2013, ApJ, 778, 143
Pesnell, W. D., Thompson, B. J., & Chamberlin, P. C. 2012, SoPh, 275, 3
Peter, H. 1999, ApJL, 522, L77
Reiss, M. A., Hofmeister, S. J., De Visscher, R., et al. 2015, JSWSC, 5, A23
Sainz Dalda, A., de la Cruz Rodríguez, J., De Pontieu, B., & Gošić, M. 2019, ApJL, 875, L18
Schmit, D., Bryans, P., De Pontieu, B., et al. 2015, ApJ, 811, 127
Schou, J., Scherrer, P. H., Bush, R. I., et al. 2012, SoPh, 275, 229
Tei, A., Gunár, S., Heinzel, P., et al. 2020, ApJ, 888, 42
Teplitskaya, R. B., Turova, I. P., & Ozhogina, O. A. 2007, SoPh, 243, 143
Wilcox, J. M., & Howard, R. 1968, SoPh, 5, 564
Wilhelm, K., Curdt, W., Marsch, E., et al. 1995, SoPh, 162, 189